HHS Public Access

Author manuscript

Mol Cancer Ther. Author manuscript; available in PMC 2015 June 18.

Published in final edited form as:

Mol Cancer Ther. 2014 November ; 13(11): 2595–2606. doi:10.1158/1535-7163.MCT-14-0422.

Development of Targeted Near-Infrared Imaging Agents for Prostate Cancer

Xinning Wang[1], **Steve S. Huang**[2], **Warren D.W. Heston**[3], **Hong Guo**[4], **Bing-Cheng Wang**[4], and **James P. Basilion**[1]

[1]Department of Radiology and NFCR Center for Molecular Imaging, Case Western Reserve University, Cleveland, Ohio

[2]Department of Nuclear Medicine, Cleveland Clinic, Cleveland, Ohio

[3]Department of Cancer Biology, Cleveland Clinic, Cleveland, Ohio

[4]Departments of Medicine, Pharmacology and Oncology, MetroHealth Campus, Case Western Reserve University School of Medicine, Cleveland, Ohio

Abstract

Prostate cancer is the most common noncutaneous malignancy affecting men in North America. Radical prostatectomy remains a definitive treatment for prostate cancer. However, prostate surgeries are still performed “blindly” with the extent of tumor infiltration past the margins of the surgery only being determined postoperatively. An imaging modality that can be used during surgery is needed to help define the tumor margins. With its abundant expression in prostate cancer, prostate-specific membrane antigen (PSMA) is an ideal target for detection of prostate cancer. The purpose of this study was to develop PSMA-targeted near-infrared (NIR) optical imaging probes for intraoperative visualization of prostate cancer. We synthesized a high-affinity PSMA ligand (PSMA-1) with low molecular weight and further labeled it with commercially available NIR dyes IRDy800 and Cy5.5. PSMA-1 and PSMA-1–NIR conjugates had binding affinities better than the parent ligand Cys-CO-Glu. Selective binding was measured for each of the probes in both *in vitro* and *in vivo* studies using competitive binding and uptake studies. Interestingly, the results indicated that the pharmacokinetics of the probes was dependent of the fluorophore conjugated to the PSMA-1 ligand and varied widely. These data suggest that PSMA-targeted probes have the potential to be further developed as contrast agents for clinical intraoperative fluorescence-guided surgery.

Corresponding Author: James P. Basilion, Department of Radiology, Case Western Reserve University, 11100 Euclid Avenue, Wearn Building B-42, Cleveland, OH 44106. Phone: 216-983-3246; Fax: 216-844-4987; jxb206@case.edu.

Note: Supplementary data for this article are available at Molecular Cancer Therapeutics Online (http://mct.aacrjournals.org/).

Disclosure of Potential Conflicts of Interest: No potential conflicts of interest were disclosed.

Authors' Contributions: Conception and design: X. Wang, S.S. Huang, J.P. Basilion
Development of methodology: X. Wang, H. Guo, B.-C. Wang, J.P. Basilion
Acquisition of data (provided animals, acquired and managed patients, provided facilities, etc.): X. Wang
Analysis and interpretation of data (e.g., statistical analysis, biostatistics, computational analysis): X. Wang, J.P. Basilion
Writing, review, and/or revision of the manuscript: X. Wang, S.S. Huang, W.D.W. Heston, J.P. Basilion
Administrative, technical, or material support (i.e., reporting or organizing data, constructing databases): H. Guo, J.P. Basilion
Study supervision: J.P. Basilion

Introduction

Prostate cancer is the most diagnosed cancer among men in the United States. Approximately 233,000 new diagnoses and 29,480 deaths from prostate cancer are projected in 2014 among men in the United States (1). An estimated 91% of prostate cancers detected at initial screenings are clinically localized and these patients are candidates for radical prostatectomies. However, surgery fails to halt the disease in approximately 20% of the patients who undergo radical prostatectomy and can be associated with comorbidities (2–4). The main challenge with radical prostatectomy is that it is difficult for surgeons to assess invasion of prostate cancer during surgery because it is often microscopic and “invisible” to the surgeon during the procedure. Therefore, the entire gland is removed, the extent of infiltrative disease only being revealed postoperatively by pathologic assessment of the resected tissues. Consequently, approximately 20% of prostatectomies do not achieve complete resections (positive margins identified postoperatively by pathology) resulting in more than 60% recurrence of the disease in those patients (2, 4). There is an urgent need to develop a technology that will improve the success rate for prostatectomies and simultaneously reduce surgery-related morbidities in localized cancers. Particularly useful would be an imaging technique that could be correlated with a relevant tumor biomarker.

Among the markers of prostate cancer, prostate-specific membrane antigen (PSMA) is the most well-established, highly specific prostate epithelia cell membrane antigen known. PSMA is a type II membrane protein with a molecular weight at about 110 kDa, originally identified from the human prostate cancer line LNCaP by Horoszewicz and colleagues (5–7). It is highly expressed in most prostate cancers; its expression increases progressively in higher grade cancers, metastatic diseases, and castration-resistant prostate cancer (6–11). In addition, PSMA has also been found in the neovasculature of almost all solid tumors (9, 12, 13). Unlike other prostate-specific antigens, PSMA is not secreted and is membrane bound (9). These properties make PSMA an attractive extracellular target for imaging and therapy. The only FDA-approved imaging agent for targeting PSMA in prostate cancer is ProstaScint. It consists of a murine antibody 7E11 labeled with ^{111}In (14). However, the antibody 7E11 binds to the intracellular domain of PSMA and therefore is not accessible for viable cells. A second-generation antibody, J591, which binds to the extracellular domain of PSMA, has been radiolabelled with ^{111}In, ^{90}Y, and ^{177}Lu and has demonstrated excellent binding characteristics and tumor-to-background signals in clinical trials with metastatic and castration-resistant prostate cancers (12, 15–19). A recent study has shown that ^{89}Zr-J591 can identify intraprostatic tumor foci in patients with localized disease (18). The major disadvantages of antibodies are the slow target recognition and background clearance in an appropriate time frame for diagnostic imaging and reduced utility for image-guided surgical approaches. The first small-molecule–based PSMA targeting imaging agent was reported in 2005 by Humblet and colleagues (20). Since then many small molecular PSMA-targeting imaging agents have been developed for single-photon emission tomography (SPECT), PET, and optical imaging (21–30). Among these imaging agents, the urea-based ^{18}F-DCFBC (25, 31, 32), ^{123}I-MIP-1072 (26), and ^{123}I-MIP-1095 (33) have entered into clinical trials and shown the ability to detect both bone and soft-tissue metastases in patients with prostate cancer.

Over the past decade, optical imaging has emerged as a real-time, sensitive, and noninvasive modality for visualization, localization, and measurement of bioactive molecules *in vivo*. It would be ideal to have an imaging agent selectively targeted to tumor lesions for best imaging contrast and diagnostic accuracy *in vivo*. This can be achieved by conjugation of receptor ligands to optical probes. The objective of this study is to develop PSMA-targeted near-infrared (NIR) imaging probes that can help define extraprostatic extension of prostate cancer and help differentiate tumor margins during surgery, improving prostatectomies. Recently, we have created a stable derivative of RBI-1033 (a nucleotide-based PSMA receptor ligand), EE'Amc-Ahx-dEdEdEG with increased negative charge and demonstrated its utility as a PET imaging agent (34). Here, we synthesized a similar high-affinity PSMA ligand and conjugated it to different NIR fluorophores. Our results demonstrate that these probes can bind efficiently and selectively to PSMA and that the fluorophores significantly affect the pharmacokinetic behavior of the PSMA–NIR conjugates. Overall, our agents have the potential to be further developed for diagnosis and image-guided surgery for prostate cancer.

Materials and Methods

General

(*S*)-2-(3-((*S*)-5-amino-1-carboxypentyl)ureido)pentanedioic acid (Cys-CO-Glu) was custom made by Bachem Bioscience Inc. *H*-Glu(OtBu)-OtBu was purchased from Bachem Bioscience Inc. Fmoc-Rink Amide MBHA resin, Fmoc-(*D*)Glu(OtBu)-OH, Fmoc-Lys(Mtt)-OH, Fmoc-Ahx-OH, and 2-(6-chloro-1*H*-benzotriazole-1-yl)-1,1,3,3-tetra-methylaminium hexafluorophosphate (HCTU) were purchased from Peptides International Inc. Fmoc-Glu-α-OtBu (Glu') was from Novabiochem. Fmoc-Amc-OH was from ABX Advanced Biochemical Compounds. All the other chemicals were purchased from Sigma-Aldrich Inc.

Synthesis of Glu-CO-Glu'-Amc-Ahx-Glu-Glu-Glu-Lys-NH_2 (PSMA-1)

PSMA-1 was synthesized manually using standard Fmoc chemistry. Generally, peptide was synthesized at 0.2 mmol scale starting from C-terminal Fmoc-rink amide MBHA resin. Fmoc deprotection at each cycle was carried out using 20% piperidine in DMF. Coupling reactions were carried out using 3.3 equivalents of Fmoc amino acids in DMF activated with 3.3 equivalents of HCTU and 5 equivalents of diisopropylethylamine (DIPEA) in DMF. These steps were repeated each time with an amino acid added. After the peptide sequence Fmoc-Glu'-Amc-Ahx-Glu-Glu-Glu-Lys(Mtt) was built on the resin, the Fmoc group of N-terminal amino acid Glu' was deprotected by 20% piperidine. Then, a chloroform solution containing 3 equivalents of *H*-Glu(OtBu)-OtBu mixed with 2.5 equivalents of DIPEA was prepared. The solution is then added slowly to 0.25 equivalents triphosgene in chloroform over 10 minutes at room temperature. After 15-minute incubation, the reaction mixture was mixed with Glu'-Amc-Ahx-Glu-Glu-Glu-Lys on rink amide resin preswollen in chloroform with 2.5 equivalents of DIPEA. After the reaction was complete, the resin was washed with DMF and then dichloromethane and dried. The peptide was cleaved from resin by TFA/water/triisopropylsilane (950:25:25). The cleaved peptide was purified by preparative high-performance liquid chromatography (HPLC). The products were ascertained by high-resolution matrix-assisted laser desorption/ionization mass (MALDI-MS) spectra from an

Applied Biosystem 4800 MALDI TOF/TOF Analyzer using positive ion mode. Retention time was 18.6 minutes. MALDI-MS: $C_{48}H_{74}N_{10}O_{20}$, 1,087.5 (found); 1,087.1 (calculated).

Synthesis of PSMA-1–IR800

Coupling of PSMA-1 to IRDye800cw NHS ester (Li-Cor Biosciences) was performed in DMF. Basically, 100 nmol of PSMA-1 was dissolved in 100 μL of DMF, to which 50 nmol of IRDye800cw NHS ester in DMF was added. The reaction was carried out at room temperature for 3 hours. The crude product was then purified by preparative HPLC. Yield: 67%. Retention time: 23.4 minutes. MALDI-MS: $C_{92}H_{126}N_{12}O_{34}S_4$, 2,071.8 (found); 2,072.3 (calculated)

Synthesis of PSMA-1–Cy5.5

The compound was synthesized using the same method as the synthesis of PSMA-1–IR800 using Cy5.5 NHS ester (Lumiprobe Life Science Solutions). Yield: 73%. Retention time: 39.4 minutes. MALDI-MS: $C_{86}H_{115}N_{12}O_2$, 1,651.7 (found); 1,651.8 (calculated).

HPLC was performed on a Shimadzu HPLC system equipped with a SPD-20A prominence UV/visible detector and monitored at a wavelength at 220 nm for PSMA-1 or 254 nm for PSMA-1–IR800 and PSMA-1-Cy5.5. Preparative HPLC was achieved using Luna 5μ C18(2) 100A column (250 mm × 10 mm × 5 μm; Phenomenex) at a flow rate of 3.0 mL/min. Analytical HPLC was performed using an analytical Luna 5μ C18(2) 100A column (250 mm × 4.6 mm × 5 μm; Phenomenex) at a flow rate of 1.0 mL/min. The gradient used was 5% to 55% acetonitrile against 0.1% trifluoroacetic acid over 30 minutes and then 55% acetonitrile for another 15 minutes.

Cell culture

Retrovirally transformed PSMA-positive PC3pip cells and transfection control PC3flu cells were obtained from Dr. Michel Sadelain in 2000 (Laboratory of Gene Transfer and Gene Expression, Gene Transfer and Somatic Cell Engineering Facility, Memorial-Sloan Kettering Cancer Center, New York, NY). The 2 cell lines were last checked and authenticated by Western blotting in 2014. No genetic authentication was performed. Cells were grown at 37°C and 5% CO_2 under a humidified atmosphere. Cells were maintained in RPMI-1640 medium supplemented (Invitrogen Life Technology) with 2 mmol/L L-glutamine and 10% FBS.

Partition coefficient (log *P*)

Determination of log *P* was performed by the “shake-flask method.” To a solution containing 500 μL of octanol and 500 μL of PBS (pH 7.4), 10 μL of 1 μmol/L PSMA-1–NIR was added. The resulting solution was vortexed and centrifuged at 3,000 rpm for 10 minutes. Aliquots of 100 μL were removed from the octanol and the saline phase. The absorbance of each layer was measured at 780 nm for PSMA-1–IR800 or 680 nm for PSMA-1–Cy5.5. Log *P* was calculated as the average log ratio value of the absorbance in the octanol fraction and PBS fraction from 3 samples.

Competitive binding assay

The assay was carried out as previously reported (35). Briefly, PC3pip cells (5×10^5) were incubated with different concentrations of ligands in the presence of 12 nmol/L *N*-[N-[(*S*)-1,3-dicarboxypropyl]carbamoyl]-*S*-[^{3}H]-methyl-L-cysteine (GE Healthcare Life Sciences) in a total volume of 300 μL for 1 hour at 37°C. The mixture was centrifuged at 3,000 × *g* for 5 minutes at 4°C and then washed 3 times with 500 μL of cold PBS. Finally, 4 mL of EcoLume cocktail (MP Biomedicals) was added, and radioactivity was counted by scintillation counter. The concentration required to inhibit 50% of binding is determined (IC_{50}) by GraphPad Prism 3.0.

In vitro cellular uptake studies

PC3pip and PC3flu cells were plated on coverslips at about 70% confluency. After incubating overnight to promote adherence, cells were treated with 1 μmol/L of PSMA-1–Cy5.5 or PSMA-1–IR800. After incubation for various times (5 minutes, 30 minutes, 1 hour, and 4 hours), cells were washed 3 times with PBS, fixed with 4% paraformaldehyde, counterstained with 4′,6-diamidino-2-phenylindole (DAPI), mounted with Fluor-Mount aqueous mounting solution, sealed with nail polish, and observed using Leica DM4000B fluorescence microscopy (Leica Microsystem Inc.). Blocking experiments were performed by coincubation of PC3pip and PC3flu cells with 1 μmol/L of PSMA-1–Cy5.5 or PSMA-1–IR800 and 10 μmol/L of Cys-CO-Glu for 4 hours.

Mouse tumor xenograft models

All animal procedures were performed according to Institutional Animal Care and Use Committee (IACUA)-approved protocols. Animals were fed on a special rodent diet (Harlan Laboratories, Inc.) to reduce auto fluorescence. For flank tumor xenografts, 6- to 8-week-old athymic nude mice were implanted subcutaneously with 1×10^6 of PSMA-negative PC3flu and PSMA-positive PC3pip cells in 100 μL Matrigel under the right and left upper chests, respectively. Animals were observed every other day until tumors reached at about 10 mm in diameter. Orthotopic implantation of prostate cancer was carried as previously described (36). Briefly, 6- to 8-week-old male athymic nude mice were first anesthetized by intraperitoneal injection of 200 μL of 5 mg/mL ketamine/3 mg/mL xylazine solution in 0.9% saline. The lower abdomen was open to expose the dorsolateral prostate, to which 10 to 20 μL cell suspension in PBS (5×10^7 cells/mL) was injected. The incision in the abdominal wall was closed. After 4 weeks, animals were ready for experimentation.

In vivo NIR imaging studies

Imaging was performed with the aid of the Maestro *In Vivo* Imaging System (Perkin-Elmer) with each mouse receiving 1 nmol of NIR probe in PBS through tale vein injection. Imaging was performed at different time points using the appropriate filter set (deep red filter set for PSMA-1–IR800 and yellow filter set for PSMA-1–Cy5.5). During imaging, the temperature of imaging bed was adjusted to 37°C. Mice received inhalation of isofluorane through a nose cone attached to the imaging bed. Mice were imaged over 5 days postinjection, after which, the mice were sacrificed by cervical dislocation and tissues such as liver, kidneys, tumors, heart, and bladder were harvested for *ex vivo* imaging. Fluorescent molecular tomographic

(FMT) images were obtained using the FMT2500 Device (Perkin-Elmer), and 3-dimensional reconstructions of fluorescent signals were acquired using the accompanying software, TrueQuant. Quantification of fluorescent signals was obtained by calibration of PSMA-1–IR800 and PSMA-1–Cy5.5 using the 780 and 680 nm channels, respectively. To block the binding of PSMA-1–NIR in mice, mice were coinjected with 1 nmol of PSMA-1–NIR probes and 100 nmol of ZJ-MCC-Ahx-YYYG, an analogue of PSMA-1 with similar binding affinity but with no optical probe attached (34). Mice were imaged by the Maestro Imaging System and FMT for up to 24 hours. For orthotopic mouse models, mice were imaged by the Maestro Imaging System at 4 hours after tail vein injection of 1 nmol of PSMA-IR800 or 24 hours after tail vein injection of 1 nmol of PSMA-1–Cy5.5. After the completion of the optical imaging, the mouse was euthanized, the abdomen was opened to expose the tumor, and the mouse was again imaged. Finally, tumor was harvest for *ex vivo* imaging.

Statistical analysis

To compare the data obtained from FMT, *t* test was used to analyze the data using Excel.

Results

Chemistry

All compounds were characterized by MALDI-TOF MS to confirm the structure (Supplementary Figs. S1–S3). PSMA-1 (Fig. 1) contains 3 D-glutamic acid residues to mimic the negative charges on the phosphate backbone of RBI1033 (the D-isomer was selected to improve the molecule's *in vivo* stability). A lysine was introduced at the C-terminal end of the ligand allowing future coupling with either IRDye800cw or Cy5.5. Both dyes are NIR emitting dyes and can avoid the natural background fluorescence interference of biomolecules, providing a high contrast between target and background tissues. The attachment of IRDye800 to PSMA-1 shifted its HPLC retention time from 18.6 to 23.4 minutes, whereas the attachment of PSMA-1 to Cy5.5 shifted the retention time further to 39.4 minutes (Supplementary Figs. S1–S3). The hydrophobicity of the 2 PSMA-1–NIR probes was determined by their log *P* values. PSMA-1–IR800 had a log *P* value at −2.14 ± 0.17, and PSMA-1–Cy5.5 had a log *P* value at −1.02 ± 0.23. Therefore, PSMA-1–Cy5.5 is more hydrophobic than PSMA-1–IR800, which concurred with the longer HPLC retention time of PSMA-1–Cy5.5 than PSMA-1–IR800.

Competition binding studies

To determine the binding affinity of the newly synthesized ligands, we performed competition binding studies (35). The results summarized in Table 1 show that the rationally designed PSMA-1 has a binding affinity 4.3-fold better (IC_{50} = 2.30 nmol/L) than the parent ligand Cys-CO-Glu (IC_{50} = 9.93 nmol/L). Interestingly, inclusion of IR800 further improved the IC_{50} of PSMA-1–IR800 to 1.53 nmol/L; in contrast, introduction of Cy5.5 did not show much effect to the binding affinity of PSMA-1–Cy5.5 (IC_{50} = 2.07 nmol/L).

In vitro cellular uptake results

To determine whether these new imaging probes would result in cellular binding and labeling of PSMA-expressing cells, we performed *in vitro* uptake studies. PSMA-positive

(PC3pip) or PSMA-negative (PC3flu) cells were incubated with 1 μmol/L of either PSMA-1–IR800 or PSMA-1–Cy5.5 for the indicated times, and cellular uptake was monitored using fluorescence microscopy. Figure 2 shows typical fluorescence images of PC3pip and PC3flu cells after incubation with PSMA-1–IR800 (Fig. 2A) or PSMA-1–Cy5.5 (Fig. 2B). Fluorescence in PC3pip cells was observed as early as 15 minutes after treatment with PSMA-1–IR800 or PSMA-1–Cy5.5 and continued to increase for 1 hour reaching a plateau thereafter. The internalized PSMA-1–NIR conjugates showed a distinct perinuclear punctate localization. In contrast to the PC3pip cells, no uptake of fluorescence was observed in PC3flu cells, even after 4 hours of incubation. To test whether the binding of PSMA-1–labeled probes to cells was specific, the cells were coincubated with each probe and a 10-fold excess of Cys-CO-Glu. It was found that the fluorescence in PC3pip cells was completely competed by coincubation with Cys-CO-Glu, indicating that binding of PSMA-1–IR800 and PSMA-1–Cy5.5 were selective for the PSMA receptor expressed on the cells.

NIR imaging results

To evaluate the *in vivo* behavior of our PSMA-1–labeled probes, mice bearing both PSMA-positive PC3pip and PSMA-negative PC3flu tumors were used. The NIR probe was injected through a tail vein injection, and mice were imaged at the designated time points by both Maestro and FMT imaging devices. When mice were injected with PSMA-1–IR800, increased uptake in PSMA-positive PC3pip tumor was observed as early as 5 minutes post-injection (Fig. 3A). The signal in PC3pip tumors kept increasing, reaching a peak at 4 hours postinjection and then gradually declined. At early time points, the signals from the mouse bladders were very strong but not retained, becoming minimal at later time points, suggesting that the PSMA-1–IR800 probe was mainly excreted from the urinary tract. Five days postinjection, mice were sacrificed, and organs were harvested for *ex vivo* imaging. Bright fluorescent signal was observed in PC3pip tumors; some signal was observed in mouse kidneys but was much lower than that in PC3pip tumors; signals in other organs and tissues including PC3flu tumors were minimal (Fig. 3B). To determine whether the *in vivo* selectivity of the probe binding was retained in animal studies, we also performed an *in vivo* competition assay. Mice were injected with 1 nmol PSMA-1–IR800 and a 100-fold excess of a competitor (Fig. 3C). These studies showed little to no uptake of the PSMA-1–IR800 probe at any time points indicating effective competition and selectivity of probe binding and retention by the tumors *in vivo.* Immediately following *in vivo* Maestro imaging, mice were imaged by FMT to get 3-dimensional (3D) quantification of the probes (Fig. 3D). The FMT data indicated that at 4 hours postinjection, the amount of PSMA-1–IR800 in PC3pip tumors (71.2 ± 14.4 pmol, 7.12% of injected dose) was significantly higher than that in PC3flu tumors (7.5 ±1.8 pmol, 0.75% of injected dose; $P = 0.0014$) and also demonstrated the effectiveness of the *in vivo* competitor to reduce PSMA-1–IR800 binding.

When mice were injected with 1 nmol of PSMA-1–Cy5.5, selective uptake in PSMA-positive PC3pip tumor was initially observed 4 hours postinjection; the signal intensity in PC3pip tumors reached their greatest values 24 hours postinjection and then remained virtually unchanged for 120 hours (Fig. 4A). FMT 3D quantification of the signals in the tumors indicated that at 24 hours postinjection, the amount of PSMA-1–Cy5.5 in PC3pip

tumors (50.8 ± 2.6 pmol, 5.08% of injected dose) was more than 10-fold higher than that in PC3flu tumors (4.5 ± 0.8 pmol, 0.45% of injected dose; $P = 0.0017$; Fig. 4D). The excellent selectivity of PSMA-1–Cy5.5 was also demonstrated by *ex vivo* imaging of removed organs, in which the signals in PC3pip tumor were significantly higher than in other organs including the kidneys (Fig. 4B). *In vivo* competition studies indicated that PSMA-1–Cy5.5 selectively bound PSMA receptors *in vivo* as little to no uptake was measured when the probe was injected with an excess of PSMA competitor (Fig. 4C and D).

To further demonstrate the utility of the new PSMA-1–NIR conjugates, we tested whether these agents were able to recognize PSMA-expressing tumors that were orthotopically implanted into the prostate capsule of male mice (Fig. 5). Mice were euthanized at 4 hours after injection of 1 nmol of PSMA-1–IR800 or 24 hours postinjection of 1 nmol PSMA-1-Cy5.5. The mouse abdomen was opened to expose the tumor for imaging. Significant fluorescent signal was taken up by the tumor, whereas little fluorescence was observed in the surrounding tissues for both PSMA-1–IR800 (Fig. 5A and D) and PSMA-1–Cy5.5 (Fig. 5G and J). *Ex vivo* imaging of the PC3pip tumor demonstrated comparable fluorescent signal with that obtained by *in vivo* imaging (Fig. 5B, C, E, and F for PSMA-1–IR800 and Fig. 5H, I, K, and L for PSMA-1–Cy5.5). These data confirmed that PSMA-1–IR800 and PSMA-1–Cy5.5 can selectively recognize and bind to orthotopic PC3pip tumors.

Discussion

The purpose of this study was to develop PSMA-targeted NIR imaging agents to help identify prostate tumors. We have synthesized a urea-based PSMA ligand (PSMA-1) and identified 2 NIR molecular imaging probes for noninvasive selective detection of tumors expressing PSMA in live animals. The ligand PSMA-1 reported here is a new urea-based PSMA ligand rationally designed on the basis of our previous structure–activity relationship studies of a 2-5A–based PSMA analogue, RBI1033 (35, 37). PSMA-1 demonstrated improved binding affinity (IC_{50} = 2.30 nmol/L) to PSMA receptor compared with the parent ligand Cys-CO-Glu (IC_{50} = 9.93 nmol/L) as determined by a competition binding assay.

A major concern of conjugation of a bulky dye to the ligand is that the dye might significantly interfere between the interaction of the ligand and receptor, causing loss of binding affinity. This, however, was not the case for these compounds. PSMA-1–IR800 and PSMA-1–Cy5.5 showed comparable or even improved binding affinity to the PSMA receptor compared with the unlabeled PSMA-1 itself. We hypothesize that the fluorophore conjugated to a long peptide linker of glutamate may exploit both the S1 and S1′ regions of the PSMA-binding site by positioning the large fluorophores outside of the 20 Å long substrate-binding pocket (S1) of PSMA (38, 39) reducing any steric hindrance and increasing binding affinity by exploiting the glutamate-binding region. *In vitro* cellular uptake experiments with PSMA-1–IR800 and PSMA-1–Cy5.5 showed that it can selectively bind to and be taken up by PSMA-expressing PC3pip cells but not by cells that do not express PSMA, that is, PC3flu cells. In the presence of excess amount of Cys-CO-Glu, the binding of PSMA-1–IR800 and PSMA-1–Cy5.5 to PC3pip cells was competed, indicating the binding is specific to the PSMA receptor. It has been found that the PSMA or PSMA–antibody complex undergoes internalization through clathrin-coated pits, closely resembling

that of transferrin receptor internalization pathway, a receptor with which the PSMA receptor has a high degree of homology (40). Our results showed that our PSMA-1–NIR probes are internalized into the cells forming a punctate accumulation in the perinuclear region, suggesting that PSMA is localized to the recycling endosome (41). The internalization of our low molecular weight ligand PSMA-1 also suggests that PSMA-1 may serve as a putative ligand for the PSMA receptor to substitute for antibodies not only for imaging but also for targeted therapeutic approaches, creating options such as the use of toxin or drug conjugates targeted to cancerous cells.

In *in vivo* experiments, both PSMA-1–IRdye800 and PSMA-1–Cy5.5 showed excellent binding selectivity to PSMA-positive PC3pip tumors with more than a 10-fold differential between PC3pip and PC3flu tumors. Interestingly, the 2 probes showed distinctively different pharmacokinetic behaviors (Supplementary Fig. S4). The amount of PSMA-1–IR800 reached its highest levels in PSMA-positive PC3pip tumors at 4 hours postinjection, whereas it took PSMA-1–Cy5.5 24 hours to reach its highest amount in PC3pip tumors. PSMA-1–IR800 was washed out relatively rapidly from the tumor, clearing in 24 to 120 hours. In contrast, *in vivo* studies with PSMA-1–Cy5.5 demonstrated that the probe remained tumor associated and virtually unchanged 5 days after administration. To understand this, we compared the structure of each fluorophore in the PSMA-1–NIR probes, which are otherwise virtually identical. IRDye800 contains 3 more negatively charged sulfate groups than Cy5.5. Therefore, PSMA-1–Cy5.5 is less polar and much more hydrophobic (log $P = -1.02$) than IRDye800 (log $P = -2.14$), and this difference may be responsible for the vastly different pharmacokinetics of the 2 PSMA-1–NIR probes. Other studies where fluorophores of intermediate polarity to IRDye800 and Cy5.5 were conjugated to PSMA-1 showed still different *in vivo* kinetics (data not shown), suggesting that polarity of the fluorophore might dramatically influence pharmacokinetics of the agents. The phenomenon that a particular NIR dye can affect the pharmacokinetics of a conjugated probe was also reported by Chen and colleagues (30). They observed that more hydrophobic probe has longer retention time in the body, consistent with our findings.

To further demonstrate that binding of our PSMA-1–NIR probes are specific for PSMA *in vivo*, competition studies were conducted by coinjection into the mice both PSMA-1–NIRs and a 100-fold excess of ZJ-MCC-Ahx-YYYG, a high affinity binder to the PSMA receptor (34). We first tried these studies using Cys-CO-Glu or PSMA-1 but were unable to achieve effective competition using up to a 1,000-fold excess of Cys-CO-Glu or PSMA-1. This is likely due to the rapid clearance from the body measured for Cys-CO-Glu (25) which may also be the case for the underivatized PSMA-1. We therefore conducted the *in vivo* competition studies using the more hydrophobic ligand ZJ-MCC-Ahx-YYYG. Using this agent, we were able to measure strong and significant displacement of the PSMA-1–NIRs (Figs. 3C and D and 4C and D). For example, in competition studies with PSMA-1–Cy5.5 and a 100-fold excess of ZJ-MCC-Ahx-YYYG, the amount of PSMA-1–Cy5.5 in PC3pip tumor decreased from 50.8 ± 2.6 pmol/g to 5.4 ± 5.74 pmol/g ($P = 0.0018$), demonstrating that approximately 90% of PSMA-1–Cy5.5 in PC3pip tumors was competed. In contrast, the amount of PSMA-1–Cy5.5 in PC3flu tumors remained unchanged (4.27 ± 0.98 pmol/g compared with 4.51 ± 0.77 pmol/g, $P = 0.454$). Similar results were obtained for the

competition studies with PSMA-1–IR800, in which more than 95% PSMA-1–IR800 in PC3pip tumors was displaced ($P = 0.0003$). These results again suggest that high PC3pip tumor uptake of the PSMA-1–NIRs is due to PSMA-specific binding.

Since the discovery of PSMA, a wide variety of imaging agents targeting PSMA have been reported. A majority of them are radiopharmaceuticals, but noninvasive optical agents are also presented. Humblet and colleagues synthesized the first phosphoramidate-IRDye78 (GPI-78) conjugate with a binding affinity at $K_i = 9$ nmol/L, but GPI-78 was cleared too fast from the body, and imaging had to be performed 20 seconds postinjection resulting in very low tumor signals (20). Liu and colleagues reported a Cy5.5-labeled phosphoramidate peptidomimetic PSMA ligand Cy5.5-CTT-54.2 with IC_{50} at 0.55 nmol/L (42). This probe demonstrated the ability to specifically label PSMA-positive prostate cancer cells, but no further *in vivo* imaging data were reported. Nakajima and colleagues synthesized an activatable J591–ICG conjugate with high specificity to PSMA; however, it took 2 days to be sufficiently activated and taken up by the tumor (43).

Recently, Chen and colleagues reported high PSMA-specific uptake *in vivo* with 800CW-2-, 800CW-3-, Cy7-2-, and Cy7-3–labeled probes (30), however, a direct comparison of binding affinity of these agents with our compounds cannot be made as K_i of these conjugates for NAALADase activity of the PSMA receptor were reported instead of binding affinity. In this work, Chen and colleagues reported imaging, uptake, and biodistribution results up to 24 hours postinjection for optical imaging probes and noted that the linker chemistry and the fluorophore both can affect the pharmacokinetics of the probes. In our study, we measured the uptake of the conjugates during an elongated time course and demonstrated significant differences in probe pharmacokinetics that were fluorophore-dependent and long-lived. Given the large impact of the fluorophore on the pharmacokinetics of these agents, full pharmacokinetic studies are important for the determination of the best way to use the imaging agents. Overall our probes show favorable pharmacokinetic behavior, fast tumor accumulation, and rapid clearance compared with the antibody-based J591–ICG conjugate and suggest a future potential of developing these agents for optical imaging of prostate cancer.

In cancer surgery, it is of utmost importance to exactly identify the extent of malignancy because the presence or absence of tumor cells after surgical removal is a decision factor in determining the therapeutic approach and the success of said therapy. Radiological techniques such as X-ray, CT, and MRI have been considered in assisting surgery, but these are not very useful for intraoperative application. While SPECT (44, 45) is possible to be used intraoperatively, patients and the surgeons will be exposed to the danger of ionizing radiation. In contrast, fluorescent imaging can provide real-time imaging during surgery, improving detection of tumors tissues and more radical removal of tumor tissues without radiation exposure. Indocyanine green (ICG) is one of the first fluorescent dyes tested for intraoperative application in glioma surgery (46). It has also shown promise in intraoperative sentinel lymph node mapping (47). The combination of optical imaging technologies with tumor-targeting strategies can shift the paradigm of surgical oncologic imaging, offering the unique opportunity to intraoperatively detect and quantify tumor growth and intraabdominal spread. Notably, fluorescent imaging probes have recently been successfully applied for the

intraoperative detection of ovarian cancer. Recently, *Nature Medicine* describes the first use of intraoperative, tumor-specific, folate receptor–targeted fluorescence imaging to highlight the precise position of small groups of cancer cells in women with ovarian cancer, thereby allowing the surgeon to carefully excise these small groups of cells (48).

For prostate cancer removal, a modality to guide surgery will be extremely useful due to the complicated structure of the prostate gland. The prostate is surrounded by many nerves and sphincter urethrae muscle fibers, which control different excretory and erectile functions. It has been shown that significant side effects can result from radical surgery, including genitourinary, gastrointestinal, and sexual dysfunction (49). The ideal fluorescent imaging agent for intraoperative use should be able to help surgeons (i) accurately define tumor spread and determine the aggressiveness of the surgical intervention in real-time, for example, determine whether the cavernous nerves need to be removed or could be spared during surgery and (ii) avoid leaving behind the cancerous tissue that is commonly associated with pathologically positive surgical margins. We have tried an IRDye800-labeled PSMA-targeting conjugate on mice bearing PC3pip flank tumors using a Da Vinci system for robotic surgery, and negative surgical margins were obtained for all excised PC3pip tumors (50) underscoring the potential impact of this technology. The 2 probes reported here have prolonged uptake in PSMA-positive tumors, especially PSMA-1–Cy5.5, and therefore may be more suitable for combination with the Da Vinci System intraoperative image-guided surgery. In the future, we will combine this technology with targeted therapeutics that will allow “clean up” of cancerous tissues that might not be accessible to the surgeons' scalpel.

Conclusion

In summary, a peptide-based highly negatively charged PSMA ligand was designed and 2 PSMA-targeting NIR probes were synthesized on the basis of the new ligand. The molecules were evaluated *in vitro* and *in vivo*. Both probes demonstrated high binding affinity and selectivity for PSMA on PC3pip tumors. Our data suggested that the 2 NIR probes reported here have the ability to effectively distinguish between PSMA-expressing and nonexpressing tumors and other tissues. They have the potential to aid in the diagnosis of prostate cancer. Importantly, it may also have the potential to reshape standard prostatectomies. In the future, probes like these will enable surgeons to identify extracapsular disease, which is currently invisible during prostatectomy, decide whether surgical removal is possible, allow discrimination between diseased, normal, and neural tissues preventing significant morbidities and result in improved patient outcome.

Supplementary Material

Refer to Web version on PubMed Central for supplementary material.

Acknowledgments

The authors thank the laboratory of Dr. John Crabb at the Cole Eye Institute, Cleveland Clinic (Cleveland, OH) for assistance with mass spectrometry.

Grant Support: The study was supported by the National Foundation of Cancer Research to J.P. Basilion.

References

1. Siegel R, Ma J, Zou Z, Jemal A. Cancer statistics, 2014. CA Cancer J Clin. 2014; 64:9–29. [PubMed: 24399786]
2. Theiss M, Wirth MP, Manseck A, Frohmuller HG. Prognostic significance of capsular invasion and capsular penetration in patients with clinically localized prostate cancer undergoing radical prostatectomy. Prostate. 1995; 27:13–7. [PubMed: 7603912]
3. Swanson GP, Lerner SP. Positive margins after radical prostatectomy: implications for failure and role of adjuvant treatment. Urol Oncol. 2013; 31:531–41. [PubMed: 21775170]
4. Wright JL, Dalkin BL, True LD, Ellis WJ, Stanford JL, Lange PH, et al. Positive surgical margins at radical prostatectomy predict prostate cancer specific mortality. J Urol. 2010; 183:2213–8. [PubMed: 20399459]
5. Horoszewicz JS, Kawinski E, Murphy GP. Monoclonal antibodies to a new antigenic marker in epithelial prostatic cells and serum of prostatic cancer patients. Anticancer Res. 1987; 7:927–35. [PubMed: 2449118]
6. Israeli RS, Miller WH Jr, Su SL, Powell CT, Fair WR, Samadi DS, et al. Sensitive nested reverse transcription polymerase chain reaction detection of circulating prostatic tumor cells: comparison of prostate-specific membrane antigen and prostate-specific antigen-based assays. Cancer Res. 1994; 54:6306–10. [PubMed: 7527294]
7. Tasch J, Gong M, Sadelain M, Heston WD. A unique folate hydrolase, prostate-specific membrane antigen (PSMA): a target for immunotherapy? Crit Rev Immunol. 2001; 21:249–61. [PubMed: 11642607]
8. Mannweiler S, Amersdorfer P, Trajanoski S, Terrett JA, King D, Mehes G. Heterogeneity of prostate-specific membrane antigen (PSMA) expression in prostate carcinoma with distant metastasis. Pathol Oncol Res. 2009; 15:167–72. [PubMed: 18802790]
9. Troyer JK, Beckett ML, Wright GL Jr. Detection and characterization of the prostate-specific membrane antigen (PSMA) in tissue extracts and body fluids. Int J Cancer. 1995; 62:552–8. [PubMed: 7665226]
10. Ross JS, Sheehan CE, Fisher HA, Kaufman RP Jr, Kaur P, Gray K, et al. Correlation of primary tumor prostate-specific membrane antigen expression with disease recurrence in prostate cancer. Clin Cancer Res. 2003; 9:6357–62. [PubMed: 14695135]
11. Wang X, Yin L, Rao P, Stein R, Harsch KM, Lee Z, et al. Targeted treatment of prostate cancer. J Cell Biochem. 2007; 102:571–9. [PubMed: 17685433]
12. Chang SS, Reuter VE, Heston WD, Bander NH, Grauer LS, Gaudin PB. Five different anti-prostate-specific membrane antigen (PSMA) antibodies confirm PSMA expression in tumor-associated neovasculature. Cancer Res. 1999; 59:3192–8. [PubMed: 10397265]
13. Chang SS, O'Keefe DS, Bacich DJ, Reuter VE, Heston WD, Gaudin PB. Prostate-specific membrane antigen is produced in tumor-associated neovasculature. Clin Cancer Res. 1999; 5:2674–81. [PubMed: 10537328]
14. Wynant GE, Murphy GP, Horoszewicz JS, Neal CE, Collier BD, Mitchell E, et al. Immunoscintigraphy of prostatic cancer: preliminary results with 111In-labeled monoclonal antibody 7E11-C5.3 (CYT-356). Prostate. 1991; 18:229–41. [PubMed: 2020619]
15. Bander NH. Technology insight: monoclonal antibody imaging of prostate cancer. Nat Clin Pract Urol. 2006; 3:216–25. [PubMed: 16607370]
16. Bander NH, Milowsky MI, Nanus DM, Kostakoglu L, Vallabhajosula S, Goldsmith SJ. Phase I trial of 177lutetium-labeled J591, a monoclonal antibody to prostate-specific membrane antigen, in patients with androgen-independent prostate cancer. J Clin Oncol. 2005; 23:4591–601. [PubMed: 15837970]
17. Bander NH, Trabulsi EJ, Kostakoglu L, Yao D, Vallabhajosula S, Smith-Jones P, et al. Targeting metastatic prostate cancer with radiolabeled monoclonal antibody J591 to the extracellular domain of prostate specific membrane antigen. J Urol. 2003; 170:1717–21. [PubMed: 14532761]
18. Osborne JR, Green DA, Spratt DE, Fareedy SB, Robinson BD, Beattie BJ, et al. A prospective pilot study of (89)Zr-J591/prostate specific membrane antigen positron emission tomography in

men with localized prostate cancer undergoing radical prostatectomy. J Urol. 2013; 191:1439–45. [PubMed: 24135437]

19. Tagawa ST, Milowsky MI, Morris M, Vallabhajosula S, Christos P, Akhtar NH, et al. Phase II study of Lutetium-177-labeled anti-prostate-specific membrane antigen monoclonal antibody J591 for metastatic castration-resistant prostate cancer. Clin Cancer Res. 2013; 19:5182–91. [PubMed: 23714732]
20. Humblet V, Lapidus R, Williams LR, Tsukamoto T, Rojas C, Majer P, et al. High-affinity near-infrared fluorescent small-molecule contrast agents for *in vivo* imaging of prostate-specific membrane antigen. Mol Imaging. 2005; 4:448–62. [PubMed: 16285907]
21. Banerjee SR, Foss CA, Castanares M, Mease RC, Byun Y, Fox JJ, et al. Synthesis and evaluation of technetium-99m- and rhenium-labeled inhibitors of the prostate-specific membrane antigen (PSMA). J Med Chem. 2008; 51:4504–17. [PubMed: 18637669]
22. Banerjee SR, Pullambhatla M, Byun Y, Nimmagadda S, Green G, Fox JJ, et al. 68Ga-labeled inhibitors of prostate-specific membrane antigen (PSMA) for imaging prostate cancer. J Med Chem. 2010; 53:5333–41. [PubMed: 20568777]
23. Chen Y, Dhara S, Banerjee SR, Byun Y, Pullambhatla M, Mease RC, et al. A low molecular weight PSMA-based fluorescent imaging agent for cancer. Biochem Biophys Res Commun. 2009; 390:624–9. [PubMed: 19818734]
24. Chen Y, Foss CA, Byun Y, Byun Y, Pullambhatla M, Mease RC, et al. Radiohalogenated prostate-specific membrane antigen (PSMA)-based ureas as imaging agents for prostate cancer. J Med Chem. 2008; 51:7933–43. [PubMed: 19053825]
25. Foss CA, Mease RC, Fan H, Wang Y, Ravert HT, Dannals RF, et al. Radiolabeled small-molecule ligands for prostate-specific membrane antigen: *in vivo* imaging in experimental models of prostate cancer. Clin Cancer Res. 2005; 11:4022–8. [PubMed: 15930336]
26. Hillier SM, Kern AM, Maresca KP, Wang Y, Ravert HT, Dannals RF, et al. 123I-MIP-1072, a small-molecule inhibitor of prostate-specific membrane antigen, is effective at monitoring tumor response to taxane therapy. J Nucl Med. 2011; 52:1087–93. [PubMed: 21680691]
27. Hillier SM, Maresca KP, Femia FJ, Marquis JC, Foss CA, Nguyen N, et al. Preclinical evaluation of novel glutamate-urea-lysine analogues that target prostate-specific membrane antigen as molecular imaging pharmaceuticals for prostate cancer. Cancer Res. 2009; 69:6932–40. [PubMed: 19706750]
28. Hillier SM, Maresca KP, Lu G, Merkin RD, Marquis JC, Zimmerman CN, et al. 99mTc-labeled small-molecule inhibitors of prostate-specific membrane antigen for molecular imaging of prostate cancer. J Nucl Med. 2013; 54:1369–76. [PubMed: 23733925]
29. Kelderhouse LE, Chelvam V, Wayua C, Mahalingam S, Poh S, Kularatne SA, et al. Development of tumor-targeted near infrared probes for fluorescence guided surgery. Bioconjug Chem. 2013; 24:1075–80. [PubMed: 23642154]
30. Chen Y, Pullambhatla M, Banerjee SR, Byun Y, Stathis M, Rojas C, et al. Synthesis and biological evaluation of low molecular weight fluorescent imaging agents for the prostate-specific membrane antigen. Bioconjug Chem. 2009; 23:2377–85. [PubMed: 23157641]
31. Cho SY, Gage KL, Mease RC, Senthamizhchelvan S, Holt DP, Jeffrey-Kwanisai A, et al. Biodistribution, tumor detection, and radiation dosimetry of 18F-DCFBC, a low-molecular-weight inhibitor of prostate-specific membrane antigen, in patients with metastatic prostate cancer. J Nucl Med. 2012; 53:1883–91. [PubMed: 23203246]
32. Mease RC, Dusich CL, Foss CA, Senthamizhchelvan S, Holt DP, Jeffrey-Kwanisai A, et al. N-[N-[(S)-1,3-Dicarboxypropyl]carbamoyl]-4-[18F]fluorobenzyl-L-cysteine, [18F]DCFBC: a new imaging probe for prostate cancer. Clin Cancer Res. 2008; 14:3036–43. [PubMed: 18483369]
33. Barrett JA, Coleman RE, Goldsmith SJ, Vallabhajosula S, Petry NA, Cho S, et al. First-in-man evaluation of 2 high-affinity PSMA-avid small molecules for imaging prostate cancer. J Nucl Med. 2013; 54:380–7. [PubMed: 23303962]
34. Huang SS, Wang X, Zhang Y, Doke A, Difilippo FP, Heston WD. Improving the biodistribution of PSMA-targeting tracers with a highly negatively charged linker. Prostate. 2014; 74:702–13. [PubMed: 24615708]

35. Wang X, Tian H, Lee Z, Heston WD. Structure-activity relationships of 2′,5′-oligoadenylate analogue modifications of prostate-specific membrane antigen (PSMA) antagonists. Nucleosides Nucleotides Nucleic Acids. 2012; 31:432–44. [PubMed: 22497258]
36. Petty A, Myshkin E, Qin H, Guo H, Miao H, Tochtrop GP, et al. A small molecule agonist of EphA2 receptor tyrosine kinase inhibits tumor cell migration *in vitro* and prostate cancer metastasis *in vivo*. PLoS ONE. 2012; 7:e42120. [PubMed: 22916121]
37. Cramer H, Okicki JR, Rho T, Wang X, Silverman RH, Heston WD. 2-5A ligands–a new concept for the treatment of prostate cancer. Nucleosides Nucleotides Nucleic Acids. 2007; 26:1471–7. [PubMed: 18066809]
38. Mesters JR, Henning K, Hilgenfeld R. Human glutamate carboxypeptidase II inhibition: structures of GCPII in complex with two potent nhibitors, quisqualate and 2-PMPA. Acta Crystallogr D Biol Crystallogr. 2007; 63:508–13. [PubMed: 17372356]
39. Hlouchova K, Barinka C, Konvalinka J, Lubkowski J. Structural insight into the evolutionary and pharmacologic homology of glutamate carboxypeptidases II and III. FEBS J. 2009; 276:4448–62. [PubMed: 19678840]
40. Ghosh A, Heston WD. Tumor target prostate specific membrane antigen (PSMA) and its regulation in prostate cancer. J Cell Biochem. 2004; 91:528–39. [PubMed: 14755683]
41. Rajasekaran SA, Anilkumar G, Oshima E, Bowie JU, Liu H, Heston W, et al. A novel cytoplasmic tail MXXXL motif mediates the internalization of prostate-specific membrane antigen. Mol Biol Cell. 2003; 14:4835–45. [PubMed: 14528023]
42. Liu T, Wu LY, Hopkins MR, Choi JK, Berkman CE. A targeted low molecular weight near-infrared fluorescent probe for prostate cancer. Bioorg Med Chem Lett. 2010; 20:7124–6. [PubMed: 20947349]
43. Nakajima T, Mitsunaga M, Bander NH, Heston WD, Choyke PL, Kobayashi H. Targeted, activatable, *in vivo* fluorescence imaging of prostate-specific membrane antigen (PSMA) positive tumors using the quenched humanized J591 antibody-indocyanine green (ICG) conjugate. Bioconjug Chem. 2011; 22:1700–5. [PubMed: 21740058]
44. Vermeeren L, Valdes Olmos RA, Meinhardt W, Bex A, van der Poel HG, Vogel WV, et al. Intraoperative radioguidance with a portable gamma camera: a novel technique for laparoscopic sentinel node localisation in urological malignancies. Eur J Nucl Med Mol Imaging. 2009; 36:1029–36. [PubMed: 19288098]
45. Sanchez F, Fernandez MM, Gimenez M, Benlloch JM, Rodríguez-Alvarez MJ, García de Quirós F, et al. Performance tests of two portable mini gamma cameras for medical applications. Med Phys. 2006; 33:4210–20. [PubMed: 17153400]
46. Haglund MM, Berger MS, Hochman DW. Enhanced optical imaging of human gliomas and tumor margins. Neurosurgery. 1996; 38:308–17. [PubMed: 8869058]
47. Colen RR, Kekhia H, Jolesz FA. Multimodality intraoperative MRI for brain tumor surgery. Expert Rev Neurother. 2010; 10:1545–58. [PubMed: 20945538]
48. van Dam GM, Themelis G, Crane LM, Harlaar NJ, Pleijhuis RG, Kelder W, et al. Intraoperative tumor-specific fluorescence imaging in ovarian cancer by folate receptor-alpha targeting: first in-human results. Nat Med. 2011; 17:1315–9. [PubMed: 21926976]
49. Talcott JA, Rieker P, Clark JA, Weeks JC, Beard CJ, Wishnow KI, et al. Patient-reported symptoms after primary therapy for early prostate cancer: results of a prospective cohort study. J Clin Oncol. 1998; 16:275–83. [PubMed: 9440753]
50. Laydner H, Autorino R, Isac W, Khalifeh A, Panumatrassamee K, Kassab A, et al. Robotic retroperitoneal transvaginal natural orifice translumenal endoscopic surgery (NOTES) nephrectomy: feasibility study in a cadaver model. Urology. 2012; 81:1232–7. [PubMed: 23541230]

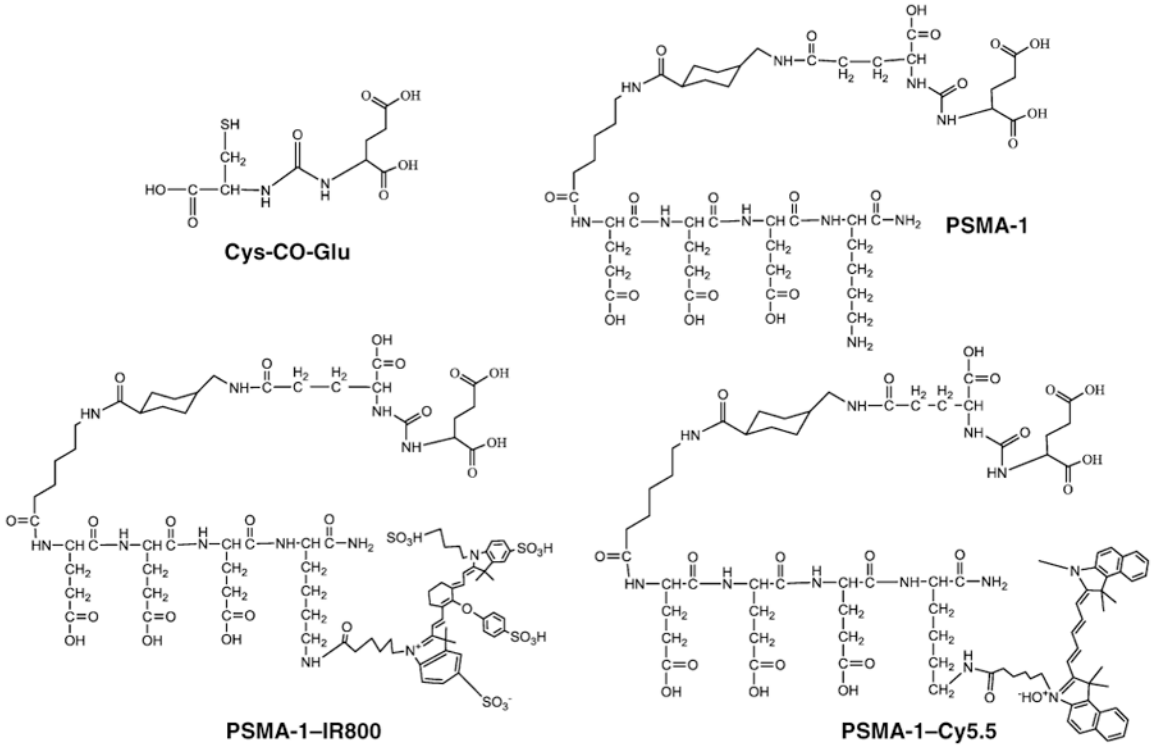

Figure 1.

Structures of PSMA ligands and PSMA–NIR conjugates. D-isomers of glutamic acid were used in PSMA-1 to provide better *in vivo* stability. IRDye800 and Cy5.5 are conjugated to PSMA-1 through the γ-NH_2 group of C-terminal lysine.

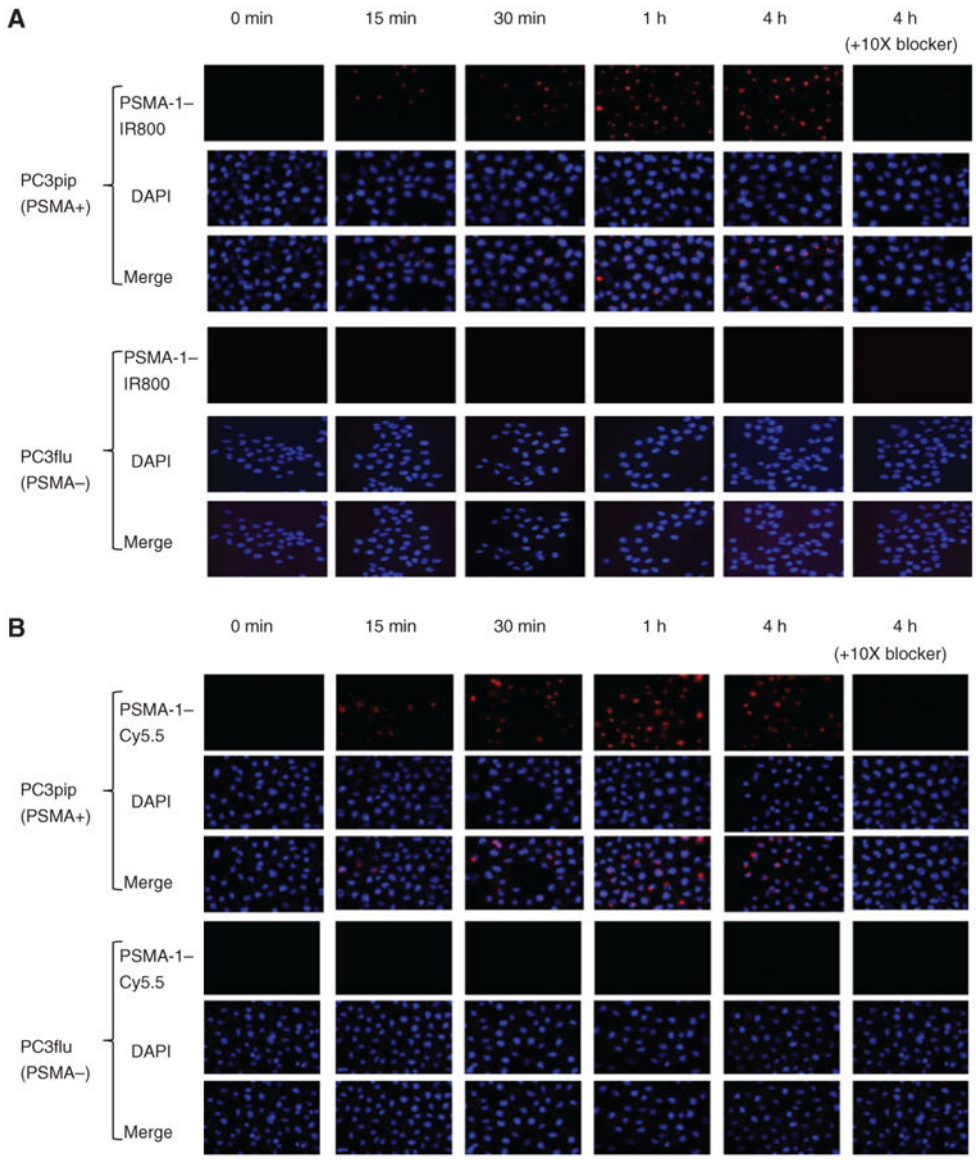

Figure 2.

In vitro cellular uptake results of PSMA-1–IR800 and PSMA-1–Cy5.5. PSMA-positive PC3pip cells and PSMA-negative cells PC3flu cells on coverslips were incubated with no probe (0 minutes, A and B) or 1 μmol/L of PSMA-1–IR800 (A) or 1 μmol/L of PSMA-1–Cy5.5 (B) for 15 minutes, 30 minutes, 1 hour, and 4 hours. The nucleus was stained by DAPI (false color blue), and uptake of PSMA-1–IR800 and PSMA-1–Cy5.5 was assessed by fluorescence microscopy (false color red). Specificity of PSMA-1–NIR conjugates to PSMA was evaluated by incubation of PC3pip and PC3flu cells with 1 μmol/L of PSMA-1–NIR conjugates and 10 μmol/L of Cys-CO-Glu, last column in each panel. Signal in PC3pip cells was significantly competed by Cys-CO-Glu, suggesting that the binding of PSMA-1–IR800 and PSMA-1–Cy5.5 to PSMA is specific. Images are taken at 40×. Representative images are shown from 3 independent experiments.

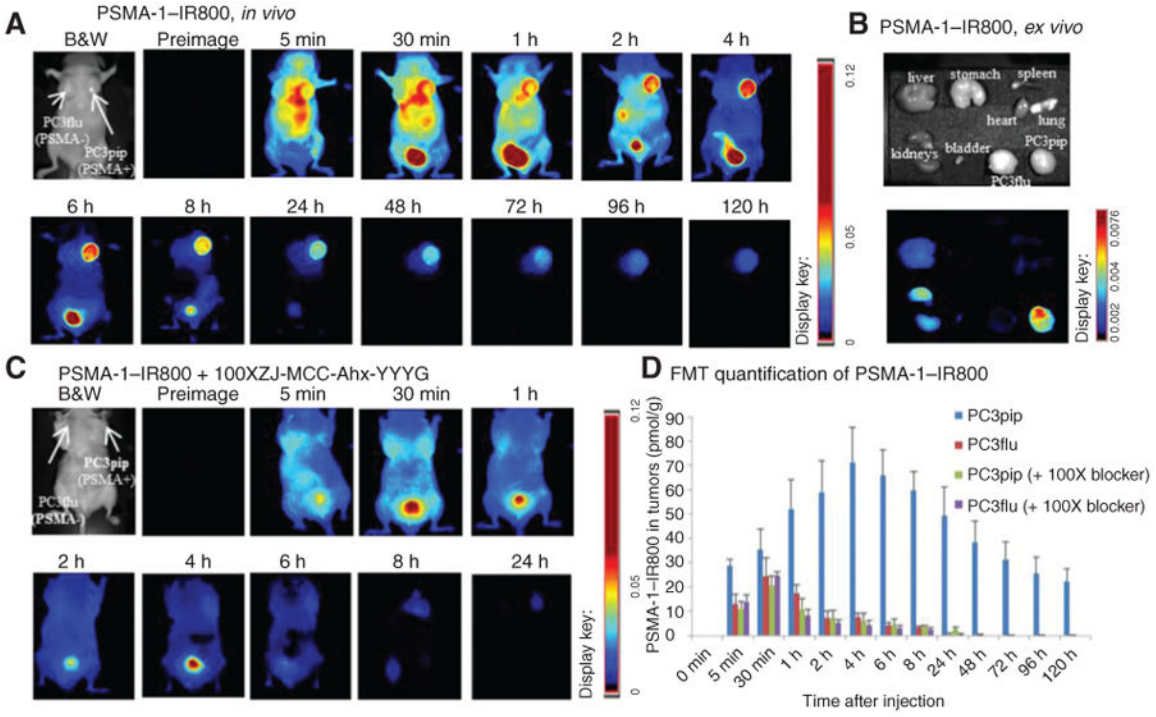

Figure 3.

Imaging of PSMA-1–IR800 in mice bearing flank PC3pip and PC3flu tumors. A, *in vivo* Maestro imaging of a typical mouse treated with PSMA-1–IR800. Mice received 1 nmol of PSMA-1–IR800 via tail vein injection and then were imaged at the designated times. Representative images are shown of $n = 5$. B, *ex vivo* imaging of mice organs at 120 hours postinjection of PSMA-1–IR800. The fluorescent signal in PC3pip tumor was significantly higher than in other organs. C, *in vivo* Maestro imaging of mice injected with 1 nmol of PSMA-1–IR800 and 100 nmol of a selective PSMA receptor–binding molecule, ZJ-MCC-Ahx-YYYG (34). Images are on the same scale as in A. Blockade of fluorescent uptake in PC3pip tumors was observed. D, FMT 3D quantification of PSMA-1–IR800 in PC3pip and PC3flu tumors from the mice used in A and C. Values represent mean ± SD of 5 animals.

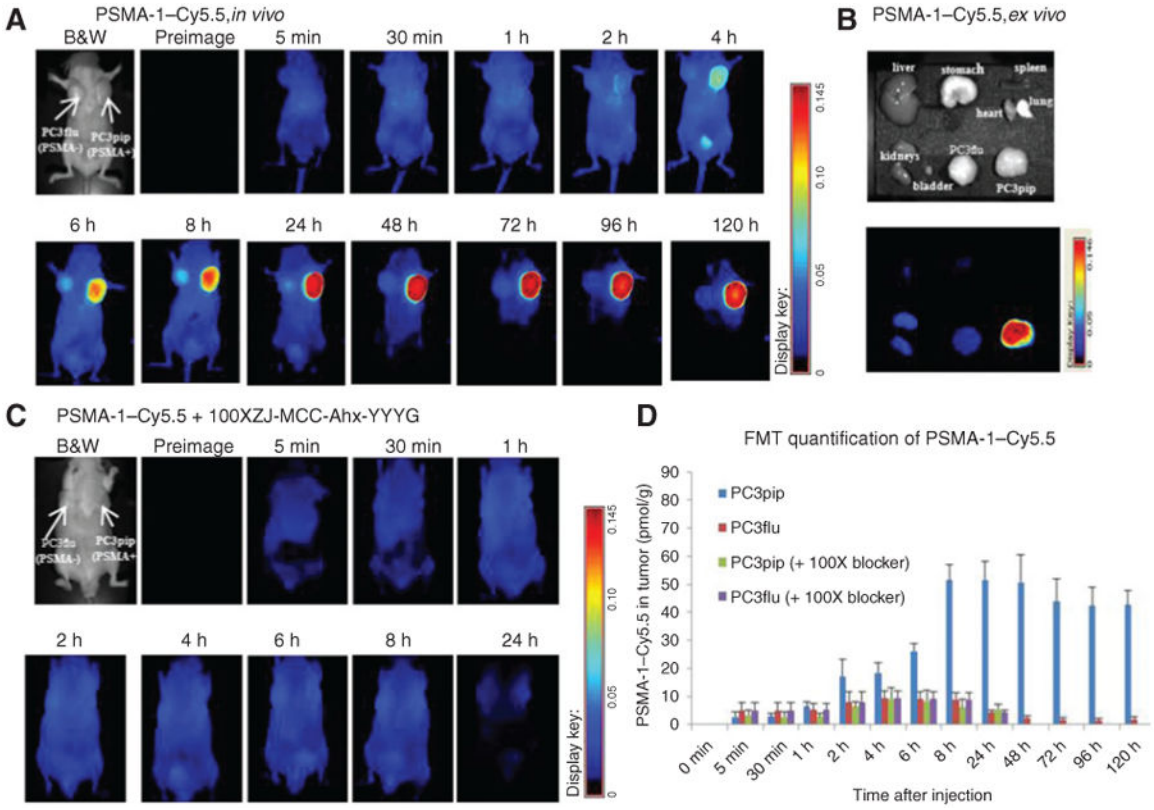

Figure 4.

Imaging of PSMA-1–Cy5.5 in mice bearing flank PC3pip and PC3flu tumors. A, *in vivo* Maestro imaging of mice treated with PSMA-1–Cy5.5. Mice received 1 nmol of PSMA-1–Cy5.5 through tail vein injection and then were imaged at the indicated times. Representative images of $n = 5$ mice are shown. Selective uptake in PC3pip tumors was observed. Highest PC3pip tumor uptake was observed 24 hours postinjection. B, *ex vivo* imaging of mice organs at 120 hours postinjection of PSMA-1–Cy5.5. The fluorescent signal in PC3pip tumor was significantly higher than in other organs. C, *in vivo* Maestro imaging of mice injected with 1 nmol of PSMA-1–Cy5.5 and 100 nmol of a selective PSMA receptor–binding molecule, ZJ-MCC-Ahx-YYYG (34). Images are on the same scale as in A. Blockade of fluorescent uptake in PC3pip tumors was observed. D, FMT 3D quantification of PSMA-1–Cy5.5 in PC3pip and PC3flu tumors from mice used in A and C. Values represent mean ± SD of 5 animals.

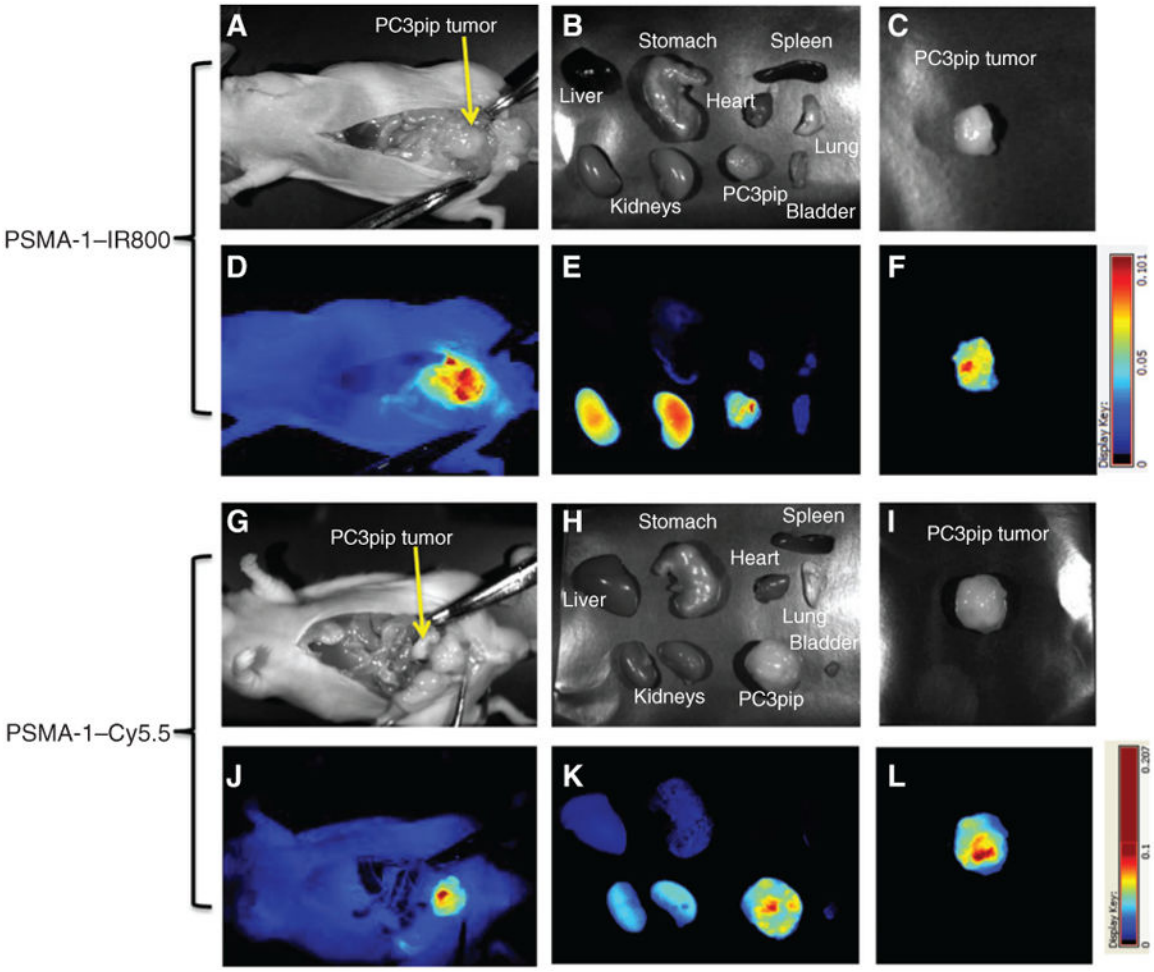

Figure 5.

PSMA-1–NIR probes can selectively target orthotopic PSMA-positive PC3pip tumors as shown by Maestro images. Mice received 1 nmol of PSMA–IR800 (A–F) or 1 nmol of PSMA-1–Cy5.5 (G–L) via a tail vein injection. Mice were sacrificed at 4 hours postinjection of PSMA-1–IR800, the abdomen opened to expose the tumor, and both black and white images (A) and fluorescent images (D) were taken. Organs were then harvested for *ex vivo* images (B and E) and finally tumors were imaged separately *ex vivo* (C and F). Mice that were administered PSMA-1–Cy5.5 were sacrificed at 24 hours postinjection; the abdomen was opened to expose tumor and then imaged. Both black and white images (G) and fluorescent images (J) were taken, organs were harvested for imaging (H and K), and finally tumors were imaged separately *ex vivo* (I and L). Pictures are representative images of 4 mice for each probe. Bright fluorescent signal was observed in PC3pip tumor.

Table 1
Summary of competitive binding results of new conjugates

	Cys-CO-Glu	PSMA-1	PSMA-1–IR800	PSMA-1–Cy5.5
IC_{50}, nmol/L	9.93 ± 0.07	2.30 ± 0.06	1.53 ± 0.14	2.07 ± 0.13

NOTE: IC_{50} is the concentration required to inhibit the binding of *N*-[*N*-[(*S*)-1,3-dicarboxypropyl]carbamoyl]-*S*-[^{3}H]-methyl-L-cysteine by 50%. Values are mean ± SD of 3 replicates.